

Influence of shear flow on the preparation of polymer layered silicate nanocomposites

Douwe Homminga^a, Bart Goderis^a, Sven Hoffman^b, Harry Reynaers^a, Gabriel Groeninckx^{a,*}

^a*Division of Molecular and Nanomaterials, Laboratory of Macromolecular Structural Chemistry, Department of Chemistry, Catholic University of Leuven, Celestijnenlaan 200F, 3001 Heverlee, Belgium*

^b*Dubble CRG/ESRF, c/o BP 220 F38043, France*

Received 14 October 2004; received in revised form 10 June 2005; accepted 19 July 2005

Available online 8 August 2005

Abstract

In this paper the influence of melt-processing on the final polymer/layered silicate nanocomposite morphology is discussed. In particular the role of shear forces on the transformation of the original large clay agglomerates is of interest. Several polymer nanocomposites were prepared by melt-extrusion, involving polycaprolactone, poly(ethylene oxide), polyamide-12 or polyamide-6 as the matrix polymer. The nanocomposite morphology was characterised by X-ray diffraction and transmission electron microscopy and the clay tactoid morphology with polarised optical microscopy and scanning electron microscopy. The development of the tactoid and nanocomposite morphology during melt-mixing under shear was studied time-resolved by optical microscopy in conjunction with a rheometer and synchrotron X-ray scattering together with a Couette type flow cell. The shear forces in the melt-preparation of polymer layered mineral nanocomposites facilitate the break-up of large-sized agglomerates, whereas the extent of further exfoliation of the mineral layers is determined by the compatibility between the polymer matrix and the mineral layers rather than by shear forces.

© 2005 Elsevier Ltd. All rights reserved.

Keywords: Polymer; Silicate; Nanocomposites

1. Introduction

Nanocomposites based on polymers and layered silicates have attracted much interest in the last decade. Numerous polymer/clay nanocomposites have been described, based on a variety of polymer matrices like for instance polycaprolactone [1–3], poly(ethylene oxide) [4,5], polyamide-12 [6,7], polyamide-11 [8], polyamide-6 [9–11], polystyrene [12], polyester [13], polyurethane [14], epoxy [15], polyvinylpyridine [16], poly(vinylidene fluoride) [17] and poly(vinylidene fluoride)/poly(methylmethacrylate) blends [17]. Polymer-layered silicate nanocomposites (PLSN) show a considerable enhancement of the strength, elastic modulus, gas barrier resistance and heat distortion temperature compared to their pure polymer counterparts

[10,18,19]. These enhancements are reached with silicate loadings as low as 1–4 vol%. The PLSN form a new fundamental scientific subject on account of the nano-scale constraints of the filler to the polymer matrix and the ultra-large specific interfacial area between the silicate and the polymer matrix.

In the early work of Toyota Research, nanocomposites were prepared by in situ polymerisation [20]. However, nanocomposites can also be generated by melt-processing [9,21–23], which for several reasons is commercially most interestingly. Accordingly, a fundamental understanding of the nanocomposite morphology formation during melt-processing is important. The main difference between melt-processing and other preparation methods is that strong shear forces act on the systems. In the present paper the influence of shear forces on the development of the nanocomposite morphology is discussed.

For a good understanding of the nanocomposite morphology it is necessary to describe the possible silicate layer organisation modes. The original clay consists of large clay agglomerates, subdivided into smaller primary clay particles that in turn are composed of a compact (face-to-

* Corresponding author. Tel.: +32 16 327440; fax: +32 16 327990.

E-mail address: gabriel.groeninckx@chem.kuleuven.ac.be (G. Groeninckx).

face) stacking or low-angle intergrowth of tactoids (crystallites). These tactoids consist of unseparated clay layer stacks. When clay is used in the preparation of nanocomposites, the silicate layers can either be present in an intercalated or an exfoliated morphology. In the former case the polymer chains are inserted in between the silicate layers, increasing the silicate long period of the stacks of the original clay structure but not destroying them. In an exfoliated morphology the silicate layers are uniformly dispersed in the polymer matrix and the stacks of the original clay structure are lost. Furthermore, the morphology of a PLSN can be a mixture of these two extreme types. In this case, individual silicate layers are present alongside intercalated clay layer stacks. In Fig. 1 a schematic overview is given of the different silicate layer arrangements [21,24]. The goal of this work is to understand the transformation of the original large clay agglomerates into the final morphology of the nanocomposite. A number of important aspects, however, have been communicated earlier by others and are summarised below.

Vaia and Giannelis state that an interplay of entropic and energetic factors determines the outcome of polymer intercalation [21,24,25]. The entropy loss associated with confinement of a polymer melt does not hamper nanocomposite formation as it is compensated by the entropy gain associated with layer separation, resulting in a net entropy change near to zero. Complete nanolayer separation needs very favourable polymer–clay interactions to overcome the penalty of polymer confinement. Furthermore, these authors concluded that polymer intercalation proceeds from the primary clay particle edges towards the particle center. Because mass transport into the primary particle was found to be the limiting step to nanocomposite formation, the

degree of constituent mixing is critical for rapid nanocomposite formation. Shear processing, such as with an ultrasonicator, parallel plate rheometer or conventional compounding equipment, will decrease the nanocomposite formation time by breaking up primary particles and establishing sample uniformity. The formation of intercalated polystyrene nanocomposites was found to take place in minutes, which made the residence time in extruders more than sufficient.

Paul et al. demonstrated that the degree of delamination and dispersion of layered silicate nanocomposites formed from polyamide-6 by melt compounding is affected by the clay chemical treatment as well as the type of extruder and its screw design. Increasing the residence time and selecting an appropriate shear history in the extruder generally improves the delamination and dispersion [9,23,26]. However, the chemical compatibility between the polymer matrix and the chemistry of the clay treatment plays the dominating role for the final morphology of nanocomposites. The shear intensity in the extruder can only decrease the tactoid particles or the size of intercalated clay stacks when the chemical compatibility is not strong enough. On the other hand, when the clay chemical treatment and the resin are compatible, almost any set of processing conditions can be used to form exfoliated nanocomposites. When the chemical treated clay and polymer are only marginally compatible, the optimisation of the process conditions determines the final morphology of the nanocomposite. However, shear forces are required to start the dispersion process by shearing particles apart into tactoids or intercalants. A residence time of a few minutes in a low or mildly shearing environment is required to allow polymer to enter the clay galleries and peel the platelets apart [23].

Relying on the conclusions formulated in the reports quoted above, one could formulate the influence of shear flow on the preparation of polymer layered silicate nanocomposites as follows. The formation of a polymer/clay nanocomposite is mostly dependent on the favourable chemical compatibility of its constituents. At sufficient compatibility the polymer can intercalate the clay layer stacks and eventually exfoliate the individual silicate layers. The role of the shear forces is merely to facilitate the intercalation process by breaking-up the original clay agglomerates and large primary clay particles into smaller sized primary clay particles.

However, in this hypothesis a number of observations is still not accounted for. When PA-6/MMT nanocomposites are prepared with a single-screw extruder a lower degree of exfoliation is found compared to when devices are used that exert stronger shear forces [23]. This indicates that the shear forces could also enhance the intercalation/exfoliation of the clay layer stacks subsequent to the initial particle break-up. Furthermore, the conclusions reached in the work by Vaia and Giannelis on the formation of the polystyrene/clay nanocomposites have validity limited to intercalated systems; the step of full exfoliation to individual silicate






Description	Morphology	Lateral size scale
Agglomerate		0.1-1 mm
Primary particles		1-10 μm
Tactoids or Crystallites		0.5-0.05 μm
Intercalated silicate layer stack		0.5-0.05 μm
Exfoliated or delaminated individual silicate layers		1-2 nm

Fig. 1. Schematic overview of the different silicate layer morphologies.

layers was not made. Therefore, the conclusions on the influence of shear forces and required residence times reached so far only apply to the first step of intercalation and not to the subsequent process of exfoliation.

To acquire a more general picture on this topic, the break-up of clay agglomerates to a final nanocomposite morphology is further discussed in this paper. The polymers polycaprolactone, poly(ethylene oxide), polyamide-12 and polyamide-6 are selected as matrix polymers since they give rise to polymer/clay nanocomposites of the different degrees of intercalation/exfoliation [1–7,9–11]. Besides the usual techniques for the study of nanocomposite morphologies, such as X-ray diffraction (XRD) and transmission electron microscopy (TEM), also polarised optical microscopy (POM) and scanning electron microscopy (SEM) were used in particular to characterise the clay tactoid morphology. Furthermore, to follow processes as a function of time during mixing under shear, optical microscopy in conjunction with a rheometer and synchrotron X-ray scattering together with a Couette type shear cell, especially designed for this kind of work, were adopted.

2. Experimental

2.1. Materials

ϵ -Polycaprolactone (PCL) (Capa 6500) with $M_w = 50,000$ g/mol was purchased from Solvay Interlox Ltd, UK, poly(ethylene oxide) (PEO) with $M_v \approx 300,000$ g/mol from Aldrich Chemical Company, Inc., USA and Polyamide-12 (PA-12) from Aldrich Chemical Company, Inc., USA. Polyamide-6 (PA-6) (Akulon K123, $M_w = 24,000$ g/mol) was kindly supplied by DSM Engineering Plastics, Sittard, The Netherlands. Montmorillonite types Cloisite 15A (dimethyl bis (hydrogenated-tallow ammonium montmorillonite) and Cloisite 30B (bis(2-hydroxy-ethyl) methyl tallow ammonium montmorillonite) were purchased from Southern Clay Products, Gonzales, USA. These MMT types will be referred to as CL15A and CL30B throughout the text.

2.2. Melt processing

Pure polymers and polymer nanocomposites were prepared by melt-mixing in a co-rotating twin-screw mini-extruder for 15 min under nitrogen atmosphere. The melt-temperatures that have been used are 80 °C for the PCL/CL15A nanocomposites, 90 °C for the PEO/CL15A nanocomposites, 220 °C for the PA-12/CL30B nanocomposites, and 250 °C for the PA-6/CL30B nanocomposites. The screw speeds were 65 tours/min for the PCL and PEO nanocomposites and 50 tours/min for the PA-12 and PA-6 nanocomposites.

PCL and PEO nanocomposites have been prepared with Cloisite 15A with loadings of 1,2,4 and 10 wt% CL15A,

respectively. PA-12 and PA-6 nanocomposites have been made using Cloisite 30B with loadings of 1,2,4 and 10 wt% CL30B, respectively.

2.3. X-ray diffraction (XRD)

X-ray diffraction measurements on PCL and PEO nanocomposites have been performed on the Dutch–Belgian Beamline (DUBBLE) at the European synchrotron radiation facility (ESRF) in Grenoble, France. The wavelength of the incident X-rays was 0.73 Å and a 2D wire chamber detector was used to collect the scattering patterns for 5 min at 1.5 m from the sample. The intensities were normalized to the intensity of the primary X-ray beam, corrected for the detector response and azimuthally averaged to 1D profiles using the Igor Pro technical computing program (Wave-metrics, USA). The scattering angles were calibrated using silver behenate and later on converted to the angles expected for Cu K_{α} -radiation for comparison with the other data sets.

Scattering patterns for PA-12 and PA-6 nanocomposites were obtained in transmission mode at room temperature with a horizontal Geigerflex diffractometer on a Rigaku Rotaflex RU-200B rotating Cu-anode (incident X-ray wavelength is 1.542 Å) at a power of 4 kW.

2.4. Transmission electron microscopy (TEM)

TEM micrographs were made on a Philips CM10, operating at 80 kV. Ultrathin sections were prepared on a Leica Ultracut ULT microtome, equipped with a Leica EM FCS cryo-unit. The samples were first trimmed with iron knives to trapezoidal shaped faces. Next, ultrathin sections (80 nm) were microtomed from these faces with a diamond knife (Drukker, International) at a sample temperature of –90 °C and a knife temperature of –75 °C. The microtomed sections were collected in a water/dimethylsulfoxide (50/50) filled boat, attached to the diamond knife. The sections were collected out of the boat on copper TEM grids (square, 300 mesh) and dried completely on filter paper.

2.5. Polarised optical microscopy (POM)

The optical microscope used was an Olympus BH-2, equipped with a digital CCD camera (JVC TK-C1381). The samples were inserted as thin films of approximately 50 μ m, melt pressed between two glass cover slips. The temperature of the samples was controlled by a Mettler FP-82HT hot stage. Data collection was triggered from the Leica Qwin Image Analysis software package.

Micrographs were taken in the melt. The melt-temperatures that have been used are 100 °C for the PCL/CL15A nanocomposites, 110 °C for the PEO/CL15A nanocomposites, 220 °C for the PA-12/CL30B nanocomposites and 250 °C for the PA-6/CL30B nanocomposites.

2.6. Scanning electron microscopy (SEM)

SEM micrographs were taken on a Philips XL-20 scanning electron microscope at an accelerating voltage of 20 kV. The samples were fractured in liquid nitrogen and the fracture surfaces etched with a suitable solvent to partially remove the polymer matrix surface. The specimens were dried for 3 days in a vacuum oven to remove remaining solvent. Finally, the fractured surfaces were sputter coated with gold in vacuum.

The etching solutions and residence times were as follows: The PCI+4% CL15A nanocomposite for 0.5–1 min in Chloroform, the PEO+4% CL15A nanocomposite for 10–30 min in a 10% ethanol solution of sodium ethoxide, the PA-12+4% CL30B nanocomposite for 1–4 h in formic acid and the PA-6+4% CL30B nanocomposite for 3–6 min in formic acid.

2.7. Optical rheometry

A ThermoHaake rheometer (Rheoscope), equipped with a microscope and digital camera, has been used to study the clay aggregate morphology under simple shear flow. Measurements were performed in rotational mode. The cone/plate configuration was used with an cone angle of 1°, a plate diameter of 70 mm and a measurement gap of 25 μm . The temperature was controlled with a K20 Lauda thermocirculator set to 95 °C. The resolution of the microscope was 1 μm .

Such measurements were performed during the mixing of PCL with approximately 4% CL15A. Component mixing without applying any shear was compared to a situation with continuous shearing at 5 s^{-1} . Optical micrographs were collected at regular intervals while recording the development of the shear stress with time.

2.8. In situ XRD under shear in a Couette system

A Couette cell developed for XRD work was constructed out of a polyimide (Vespel, Du Pont, France) and basically consists of a central stator and an outer rotor. The design resembles that of the polycarbonate cell reported earlier by others [27] but was adapted for temperature control with air-flow powered heating units for both the rotor and the stator.

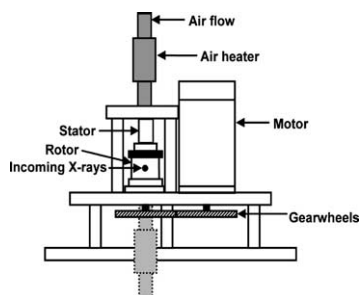


Fig. 2. Schematic of the assembled Couette cell.

A schematic of the Couette cell is shown in Fig. 2. Polyimide was chosen to replace polycarbonate because of its higher dimensional stability at elevated temperatures and its transparency to X-ray radiation.

The time-resolved XRD experiments were conducted at the Dutch–Belgian Beamline (DUBBLE) as described above but data were collected in consecutive 6 s intervals for 15–30 min.

With this set-up the mixing of PCL/CL30B and PA-12/CL30B nanocomposites was studied. Note that in the case of PCL also CL30B was chosen instead of CL15A as this clay type produces a clearer scattering peak. For the experiments the MMT powder was manually pre-mixed with the polymer granulate in a beaker. This powder was placed in the stator of the Couette cell, which was heated to the polymer melting temperature. After melting of the polymer, the outer rotor was placed on the stator and the Couette cell was further assembled to working order. After this the shutter to the X-ray beam could be opened. Unfortunately, in this way the very beginning of the mixing process, i.e. approximately 3 min, could not be captured. The mixing of PCI with 10% CL15A at 100 °C and of PA-12 with 5% CL30B at 220 °C was studied without shear and while shearing at 50 s^{-1} .

3. Results and discussion

3.1. Nanocomposite morphology

The Figs. 3–6 display the XRD curves of the PCL/CL15A, PEO/CL15A, PA-12/CL30B and PA-6/CL30B nanocomposites, respectively. The intensities of the patterns associated with the nanocomposites increase with increasing MMT content and are, therefore, easily distinguishable and can accordingly be indicated with the general term ‘nanocomposites’. The XRD-curve of pure CL15A (included in Figs. 3 and 4) shows a strong peak at $2\theta = 2.8^\circ$, corresponding to the long period of the CL15A silicate layer stacks. This corresponds to a long period of 32 Å. The

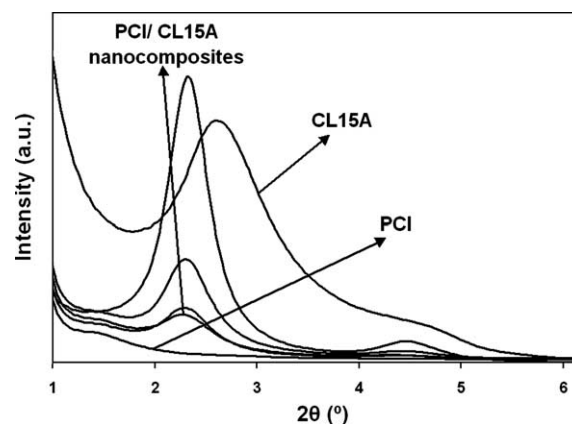


Fig. 3. XRD-patterns of PCI, CL15A and the PCI/CL15A nanocomposites.

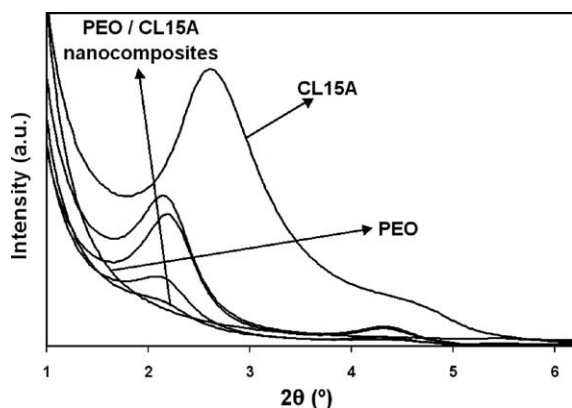


Fig. 4. XRD-patterns of PEO, CL15A and the PEO/CL15A nanocomposites.

long period is, in this case, defined as the layer-to-layer distance measured from the center of gravity of each layer. All PCL/CL15A nanocomposites exhibit a peak at $2\theta = 2.3^\circ$, independent of the MMT contents, which corresponds to a long period of 38 Å. This increase in long period compared to the original CL15A MMT clay points to the intercalation of one or two polymer chains between the silicate layers. The presence of an XRD peak indicates that the MMT morphology cannot be fully exfoliated. However, with such a peak it cannot be excluded that the morphology contains both intercalated stacks and exfoliated individual silicate layers. The same holds for the PEO/CL15A nanocomposites. In this case the MMT peaks are at $2\theta = 2.2^\circ$, corresponding to a long period of 40 Å.

The XRD-curve of pure CL30B (included in Figs. 5 and 6) shows a strong peak at $2\theta = 4.8^\circ$. This corresponds to a long period of 18 Å. The PA-12/CL30B nanocomposites irrespective of the MMT contents, exhibit peaks at $2\theta = 2.5^\circ$, corresponding a long period of 35 Å. Clearly, the peak shift is more pronounced compared to that in the PCL/CL15A and PEO/CL15A nanocomposites. So, it can be expected that the morphology of the PA-12/CL30B nanocomposites contains a substantial amount of exfoliated material but of course some intercalated stacks must be present as well. In

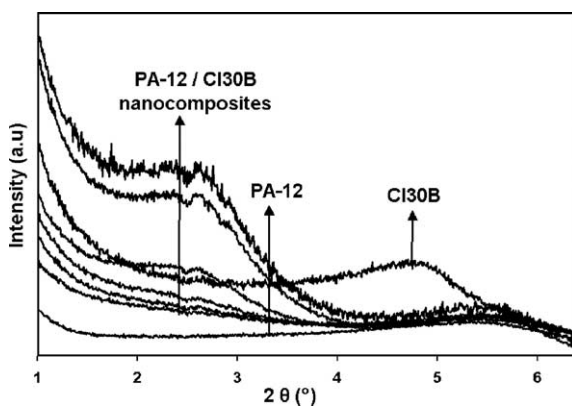


Fig. 5. XRD-patterns of PA-12, CL30B and the PA-12/CL30B nanocomposites.

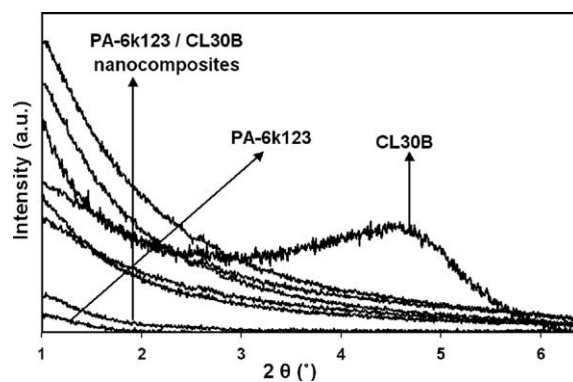


Fig. 6. XRD-patterns of PA-6, CL30B and the PA-6/CL30B nanocomposites.

contrast, MMT peaks are fully absent in all PA-6/CL30B nanocomposites pointing at a fully exfoliated dispersion of the MMT silicate layers.

TEM micrographs of PCL+4% CL15A, PA-12+4% CL30B and PA-6+4% CL30B are given in Figs. 7–9, respectively, and are representative for samples with other MMT concentration. Unfortunately, for PEO+4% CL15A no TEM micrographs are available. The micrographs confirm the XRD results. In the PCL+4% CL15A nanocomposite, the majority of the silicate layers are present as intercalated clay layer stacks. The amount of individual silicate layers is extremely low (Fig. 7). The PA-12+4% CL30B nanocomposite contains mostly individual silicate layers and only shows a few slightly thicker black lines that indicate silicate layer stacks (Fig. 8). The PA-6/CL30B nanocomposite clearly shows an almost fully exfoliated nanocomposite morphology (Fig. 9).

3.2. Tactoid morphology

Figs. 10–13 show the optical micrographs of mixtures of polymer and MMT clay in the melt. The matrix polymers in Figs. 10–13 are PCL, PEO, PA-12 and PA-6, respectively.

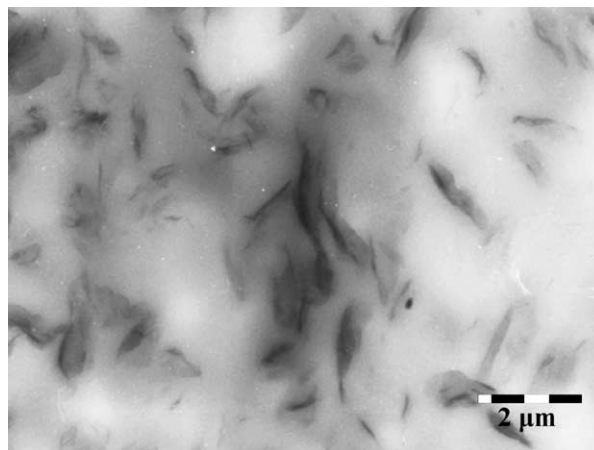


Fig. 7. Transmission electron micrograph of the PCL+4 wt% CL15A nanocomposite.

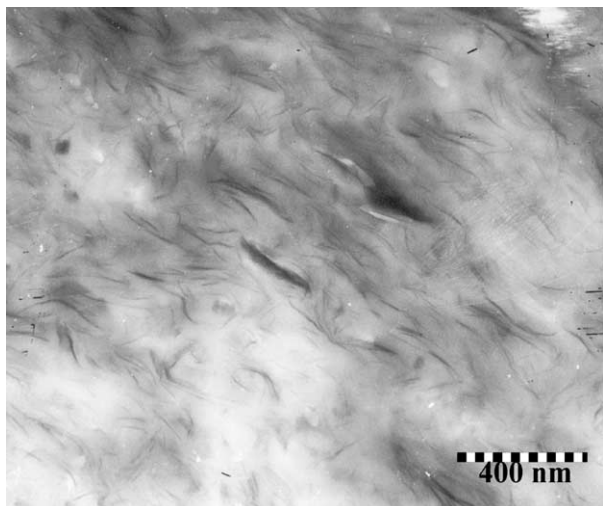


Fig. 8. Transmission electron micrograph of the PA-12+4 wt% CL30B nanocomposite.

In all figures three micrographs (a), (b) and (c) are depicted. The first micrograph (a) represents the extruded polymer nanocomposite of 4 wt% MMT after melt-extrusion as described in Section 2.2. The second micrograph (b) represents a molten mixture of polymer with 4 wt% MMT without processing. Here, the polymer and clay were manually pre-mixed in a beaker and then kept in the melt for the same time as was allowed for extrusion. The last micrograph (c) is similar to (b) but with an MMT concentration of 1 wt%.

For the PCL+4% CL15A and PEO+4% CL15A nanocomposites, the micrograph of the extruded nanocomposite (a) contains small white spherical objects about 1–2 μm in size. Apparently some micron-sized tactoids remain in the processed nanocomposites. This is in agreement with Section 3.1, where it was found that the clay in the PCL/CL15A and PEO/CL15A nanocomposites was not fully exfoliated. However, the micrographs of the unprocessed blends of polymer with the same MMT concentration (b)

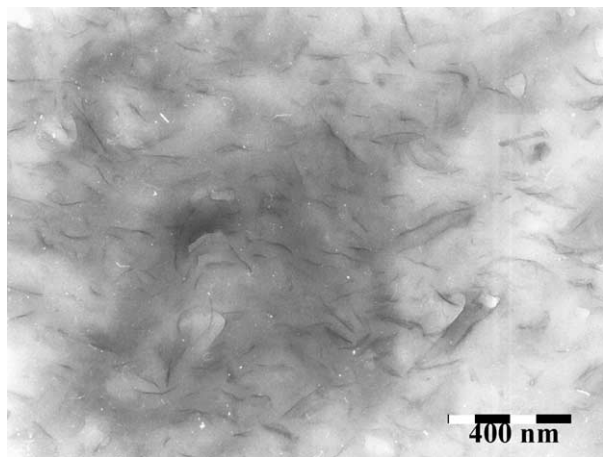


Fig. 9. Transmission electron micrograph of the PA-6+4 wt% CL30B nanocomposite.

show a much larger amount of tactoids/agglomerates of clay. So, some part of the originally added MMT must have lost its tactoid morphology and be dispersed to a sub-microsized level during melt processing. Also, it can be observed that in the unprocessed blends of polymer with MMT much larger tactoids, up to 10–20 μm in size, are present. The break-up of tactoids by the extrusion process is thus clearly demonstrated. Note that the black spots which sometimes appear in the micrographs of unprocessed blends of 4 wt% MMT concentration are local, high concentrations of MMT that fully block the microscope light beam. For comparison of the extruded and the unprocessed polymer blends without these black spots, optical micrographs of an unprocessed blend of lower (1 wt%) MMT concentration (c) is also depicted. Already at low concentrations of added MMT, a considerable amount of tactoids can be observed in the polymer melt. The amount of tactoids that can be observed in the extruded blends is less than was added originally to the blend.

For the PA-12/CL30B and PA-6/CL30B nanocomposites, the micrographs of the extruded nanocomposite (a) contain no or almost no clay tactoids. This is again in agreement with the observations in Section 3.1. The PA-6/CL30B nanocomposites are thought to be fully exfoliated, while the PA-12/CL30B nanocomposites are partially exfoliated but with a much higher level of exfoliation than the PCL/CL15A and PEO/CL15A nanocomposites. Micrographs of the unprocessed polymer blends of 4 and 1 wt% MMT, respectively, are again depicted for comparison in (b) and (c). Interestingly a high amount of micron-sized clay tactoids is present in the micrographs (b) that are absent or reduced to a smaller size after extrusion (a).

The tactoid morphology of the extruded nanocomposites has been further investigated using SEM because much smaller tactoids—when they are present—can be observed due to the higher resolution of this technique. However, it must be noted that individual silicate layers and/or small stacks of only a few silicate layers are not visible in the SEM micrographs. So, on the micrographs of samples containing only individual silicate layers, only the polymer matrix is observed. The samples used in this technique are broken polymer strands of mm-sized dimensions. The surface for examination is quite large and the composition on a micron-scale rather heterogeneous. Therefore, the micrographs that are depicted are not necessarily representative for the whole surface. Actually, places with clay tactoids are displayed selectively.

The sample surface of the PCL+4 wt% CL15A nanocomposites contained only a minor amount of clay tactoids, concentrated in small areas. In the major part of the surface, only the polymer matrix could be observed. This surface has been depicted in the micrograph of Fig. 14(a). Fig. 14(b) depicts a part of the surface with clay tactoids. From the XRD and TEM measurements it was known that the PCL+4 wt% CL15A nanocomposite was not fully exfoliated. However, the low amount of clay tactoids observed with

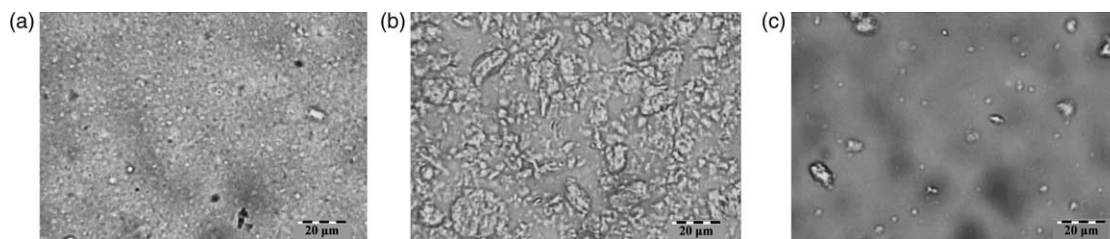


Fig. 10. Optical micrographs of the extruded PCL + 4 wt% CL15A nanocomposite (a), and the unprocessed blend of virgin PCL and 4 wt% CL15A clay (b) and the unprocessed blend of virgin PCL and 1 wt% CL15A clay.

SEM indicates that almost all clay has been dispersed to the sub-micron level. Since only a single XRD peak is observed it has to be concluded that the large and the sub-micron clay layer aggregates exhibit the same internal structure or degree of intercalation.

The sample surface of the PEO + 4 wt% CL15A nanocomposite is completely different. The whole surface is covered with 5–10 μm sized clay tactoids. This can be clearly observed in the low-resolution micrograph of Fig. 15(a). The size and shape of the clay tactoids can be examined in more detail in the high-resolution micrograph of Fig. 15(b). As for the PCL + 4 wt% CL15A nanocomposite, it was deduced for the PEO + 4 wt% CL15A nanocomposite from the XRD measurement that the nanocomposite was not fully exfoliated. However, both composites have a total different clay tactoid morphology. Although the PEO/CL15A sample is packed with large clay agglomerates comparison of the optical micrographs of processed and unprocessed PEO/CL15A blends demonstrates that also some part of the original clay has been dispersed to a submicron level during extrusion. Also here, in the XRD pattern only one shifted clay peak, associated with intercalated clay stacks, can be observed. The original CL15A clay peak of smaller long period is lost. So, apparently clay stacks can be intercalated with polymer chains without fully dissolving the clay tactoids.

The sample surface of the PA-12 + 4 wt% CL30B nanocomposites contained almost no clay tactoids. This surface is depicted in the micrograph of Fig. 16(a). After intensive investigation of the sample surface, some clay tactoids could, however, still be found. These are depicted in the micrograph of Fig. 16(b). The observations with SEM support those of the XRD and TEM measurements. The PA-12 + 4 wt% CL30B nanocomposite was found to be

partially exfoliated with a high degree of exfoliation. The very low amount of clay tactoids, as observed with SEM, is again a strong indication that the clay layers of the original clay are exfoliated to individual layers and/or small layers stacks.

The sample surface of the PA-6 + 4 wt% CL30B nanocomposites contained no clay tactoids whatsoever. This surface is depicted in the micrograph of Fig. 17. Clearly, only the polymer matrix can be observed. As was known from the XRD and TEM measurements, the PA-6 + 4 wt% CL30B nanocomposite was fully exfoliated. The absence of clay tactoids in the SEM micrographs is a further proof for the fully exfoliated morphology of the PA-6 + 4 wt% CL30B nanocomposite.

An interesting conclusion from the presented investigation on tactoid morphology is that the degree of exfoliation is correlated with a lower amount of observable clay tactoids. This is not unlogical since the exfoliation of clay to individual silicate layers automatically implies the disappearance of clay tactoids. However, in partially exfoliated or intercalated polymer nanocomposites, non-exfoliated clay is not necessarily present as clay tactoids. Another possibility could have been that the non-exfoliated clay consists exclusively of small clay layer stacks containing only a few silicate layers, which is not the case. Since shear was applied to all samples and since nevertheless different degrees of tactoid degradation can be obtained one has to conclude that the full break-up of the tactoids is not only due to the shear forces from the extrusion process. The intercalating/exfoliating ‘power’ of the polymer/clay system is also a major factor for the full break-up of clay tactoids. Only in the case of high compatibility between polymer and clay, clay tactoids are fully broken up. This is a strong indication that the role of

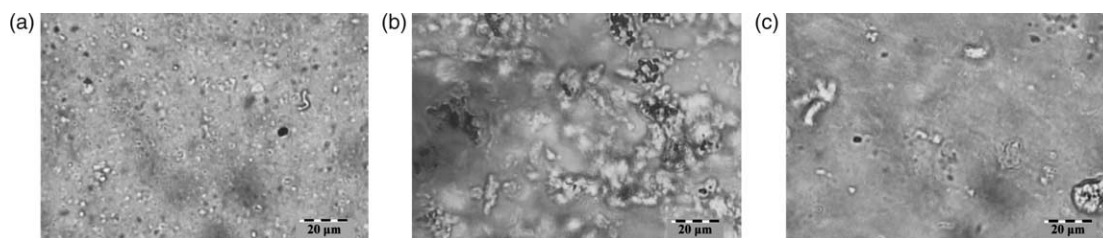


Fig. 11. Optical micrographs of the extruded PEO + 4 wt% CL15A nanocomposite (a), and the unprocessed blend of virgin PEO and 4 wt% CL15A clay (b) and the unprocessed blend of virgin PEO and 1 wt% CL15A clay.

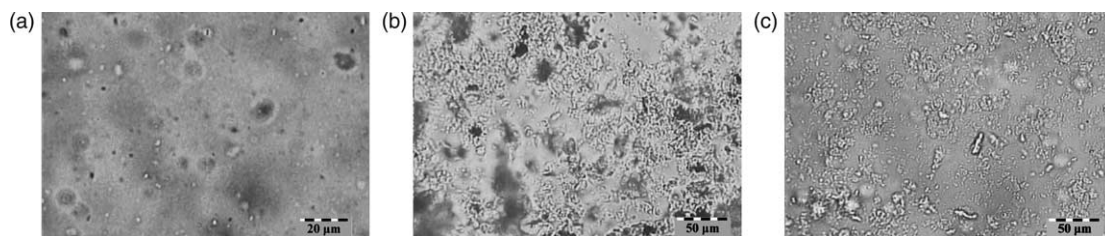


Fig. 12. Optical micrographs of the extruded PA-12 + 4 wt% CL30B nanocomposite (a), and the unprocessed blend of virgin PA-12 and 4 wt% CL30B clay (b) and the unprocessed blend of virgin PA-12 and 1 wt% CL30B clay.

the shear forces for the exfoliation of silicate layers lies only in the first break-up of the clay tactoids. Further break-up of the tactoids is apparently brought about for the major part by exfoliation of silicate layers caused by compatibility of the constituents and not through the shear forces. This is further confirmed by the fact that the clay tactoids in the different polymer nanocomposites studied, when present, have all about the same size (around 5 μm). This seems to be the limit for the break-up of clay tactoids under the influence of shear forces.

3.3. Influence of shear on tactoid break-up and nanocomposite morphology

The effect of the shear forces in the extrusion process on the break-up of the clay tactoids and the final nanocomposite morphology has been investigated with optical rheometry and in situ SAXS measurements in a shear cell.

First the polymer sample was melted on the plate of the rheoscope and later flattened by the cone. Afterwards the MMT clay was added to the melt on a specific spot to maximise the size of the original μm sized clay tactoids and hence to facilitate visualisation of their break-up. Optical images are taken at regular intervals from the melt between the glassy cone and plate of the rheometer. In Fig. 18, the rheoscope micrographs of the mixing of PCL with 4 wt% CL15A without applying shear are shown at regular 1.5 min intervals. The break-up of the very large clay tactoid into smaller pieces can easily be followed. Moreover, besides braking up the clay tactoid also ‘dissolves’ very slowly in the polymer matrix. This process starts from the borders of the clay tactoid and propagates inwards. For the ‘dissolving’ of the clay structure into the polymer matrix by intercalation/exfoliation, it needs to be accessible to the

intercalating polymer chains. As can be seen, the break-up of the clay tactoid is a rather slow process.

The rheoscope micrographs of the mixing of PCL with 4 wt% CL15A while shearing at 5 s^{-1} are depicted in Fig. 19. The clay tactoid is instantly broken up into smaller ones (lighter areas in the image taken after 1.5 min). The smaller clay tactoids are displaced with the moving polymer melt. After a few minutes, all clay tactoids seem to have disappeared. In principle, when clay tactoids are not visible anymore in the rheoscope micrographs, they can still be present at different places in the polymer melt between the cone and plate. However, the clay tactoids, if present, would reappear in the focal spot because of the continuous shear flow. As this is not the case, it can be concluded that the clay tactoids are indeed broken down to scales that are no longer accessible with an optical microscope at this time. Besides intercalating/exfoliating through polymer chains, the break-up of the clay tactoid is clearly also assisted by the applied shear forces.

These measurements give interesting information on the break-up of clay tactoids under the influence of shear forces. It must be noted, however, that the (simple) shear forces applied with the rheoscope are not comparable to the higher (complex) shear forces occurring in the extrusion process. Also, the shear rate of the experiment is taken rather low because the sharpness of the micrographs is better with lower shear rates. The brake up time accomplished by extrusion may thus even be shorter!

The influence of shear forces on the development of the nanocomposite morphology during the mixing process has also been investigated with in situ XRD under shear in a Couette cell. The scattering patterns provide information on the nanomorphology, like long period and degree of exfoliation. However, the SAXS patterns do not provide

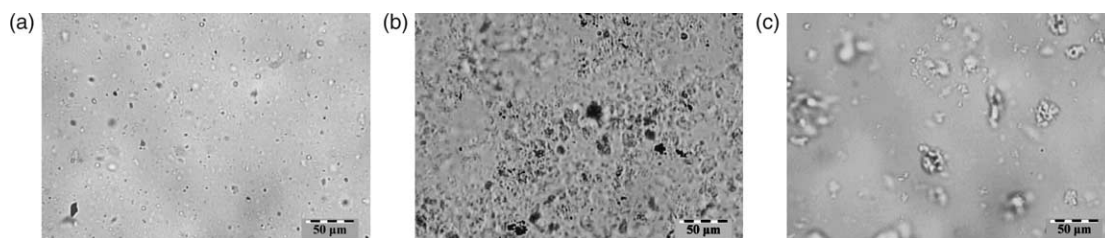


Fig. 13. Optical micrographs of the extruded PA-6 + 4 wt% CL30B nanocomposite (a), and the unprocessed blend of virgin PA-6 and 4 wt% CL30B clay (b) and the unprocessed blend of virgin PA-6 and 1 wt% CL30B clay.

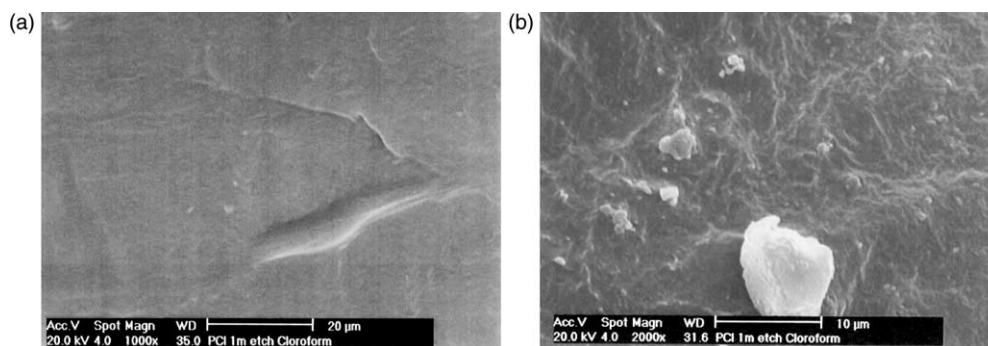


Fig. 14. Scanning electron micrographs of the PCL + 4wt% CL15A nanocomposite. The first micrograph is focussed on a location on the specimen without tactoids (a) and the second on a location with tactoids (b).

direct information about the clay tactoid morphology. The scattering patterns of the silicate layer stacks that still are arranged in the overlaying superstructure (the tactoids) are identical to the ones of stacks that are dispersed on sub-micron level. However, in a combination of the XRD Couette shear cell measurement with the optical rheoscope measurements all relevant length scales are covered.

The mixing of PCL with 10 wt% CL30B without shear and while shearing at 50 s^{-1} are depicted in Figs. 20 and 21, respectively. Note that also CL30B has been selected instead of CL15A to enhance the XRD clay peak shift. In Figs. 20(a) and 21(a), the scattered intensity is shown as a function of scattering angle and time; higher intensities are shown in black. For clarity, the same measurements are depicted in Figs. 20(b) and 21(b) as a function of scattering angle for a few selected times. For both types of mixing the peak associated with clay appears approximately at 2.3° (38 \AA). In Section 3.1 it was demonstrated that the CL30B scattering peak lies at 4.8° (18 \AA). Apparently, the intercalation/exfoliation process was already finished prior to the first actual XRD measurement. This must have happened during the three minutes that were needed to bring the sample into the Couette shear cell.

In fact, the XRD patterns shown in Fig. 20 give a confusing picture of the mixing process of PCL and CL30B without shear. At some times the scattering peak associated with clay can be seen while in other instances it cannot. The

scattering pattern taken at 15 min indicates an intercalated/partially exfoliated state while, e.g. at 9 min the absence of the scattering peak could be wrongly interpreted as an indication of full exfoliation. The problem with the measurement without shear was that the clay is not homogeneously distributed over the Couette cell. The clay tactoids float around in the polymer matrix by Brownian motion and can only be observed when they pass the narrow X-ray beam. The gap size of the Couette cell is 0.5 mm, which is much larger than the original clay tactoids. As a result and in contrast to the rheoscope set-up ($50 \mu\text{m}$ gap) clay tactoids cannot get stuck between the walls of the cell. Remember that in the rheoscope case a large tactoid could be fixed at rest. In the mixing process of PCL and CL30B with shear (Fig. 21) the scattered intensities remain the same throughout the experiment. This situation can be imagined as being due to a fast homogenisation of the system by braking up the larger particles into smaller ones. Examination of the polymer melt, after opening of the Couette shear cell directly after the measurement, confirmed this hypothesis. After the mixing process with shear, no large clay tactoids are observed and the melt is homogeneous, at least on a macroscopic scale. However, in the mixing process without shear small large clay agglomerates can be observed in the polymer melt. The shape of these clay particles is like the clay tactoids observed during the measurements in the optical rheoscope without shear

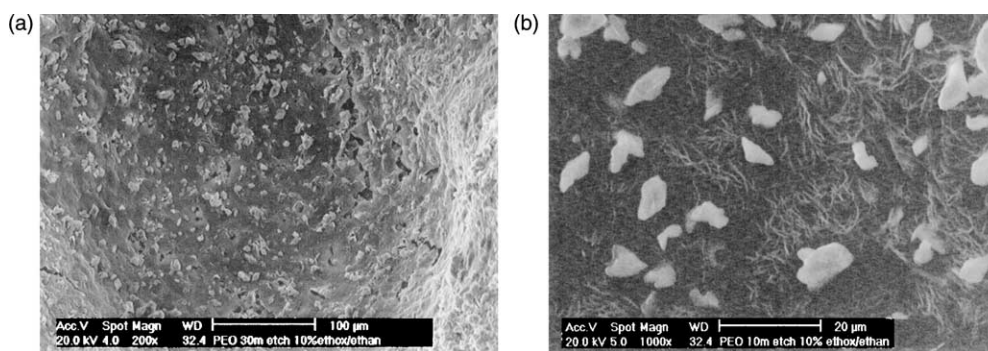


Fig. 15. Scanning electron micrographs of the PEO + 4 wt% CL15A nanocomposite. The first micrograph is taken with a low magnification (a) and the second with a higher magnification (b).

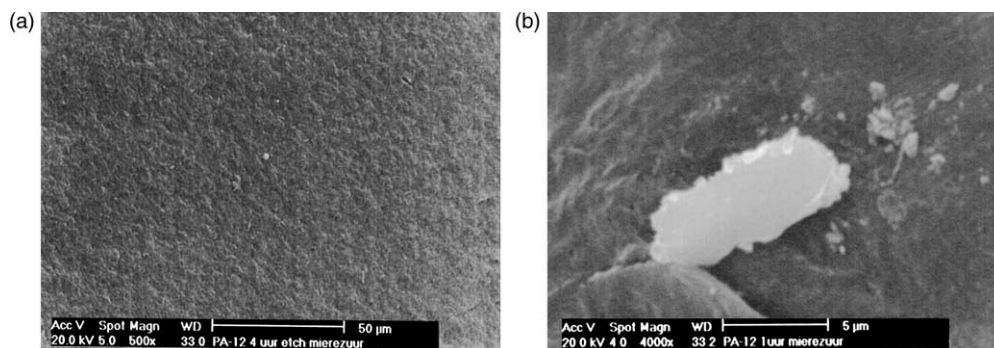


Fig. 16. Scanning electron micrographs of the PA-12 + 4 wt% CL30B nanocomposite. The first micrograph is focussed on a location on the specimen without tactoids (a) and the second on a location with tactoids (b).

(picture 18). The clay is slowly ‘dissolving’ in the polymer matrix.

The scattering patterns associated with the mixing of PA-12 with 5 wt% CL30B without shear and while shearing at 50 s^{-1} are depicted in Figs. 22 and 23, respectively. In Figs. 22(a) and 23(a), the scattered intensity is shown as a function of scattering angle and time; higher intensities are shown in black. For clarity, the same measurements are depicted in Figs. 22(b) and 23(b) as a function of scattering angle for a few selected times. For both types of mixing, the peak associated with clay appears approximately at 2.5° (35 \AA). From Section 3.1 it is known that the CL30B scattering peak lies at 4.8° (18 \AA). Again, the intercalation/exfoliation process already finished in the time before the first XRD pattern was collected, during sample insertion. The patterns taken during the mixing process of PA-12 and CL30B clay without shear shown in Fig. 22 are again influenced by the inhomogeneity of the sample in the Couette shear cell. This problem makes an unambiguous interpretation of the measurement in Fig. 22 impossible. However, investigation of the polymer melt after opening of the Couette shear cell directly after the measurement showed again the remains of small mm-sized clay agglomerates. The clay agglomerates have a zigzag edged shape, like the clay is slowly ‘dissolving’ in the polymer matrix. The mixing process of PA-12 with CL30B

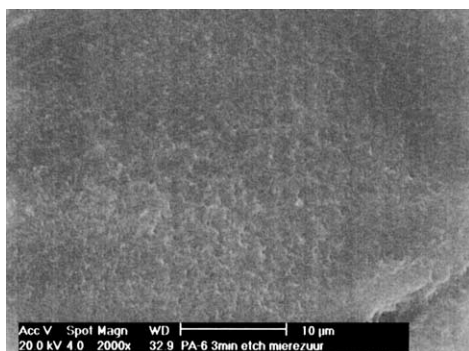


Fig. 17. Scanning electron micrographs of the PA-6 + 4 wt% CL30B nanocomposite.

clay on the scale of clay tactoids seems to take place rather slowly (more than 30 min at least, the time of the measurement).

In the mixing process of PA-12 and CL30B clay with shear (Fig. 23), the SAXS patterns do provide some interesting information. Like before, the shift of the clay peak from 4.8 to 2.5° could not be captured. However, the peak associated with the silicate layers is gradually decreasing with time at fixed angle. The slow declining of the peak associated with the clay layer stacks indicates the exfoliation of clay stacks to individual silicate layers. In a time interval of 15 min an almost fully exfoliated silicate layer structure is obtained. The exfoliation of the silicate layers after initial intercalation of the silicate layer stacks seems to be a very gradual process.

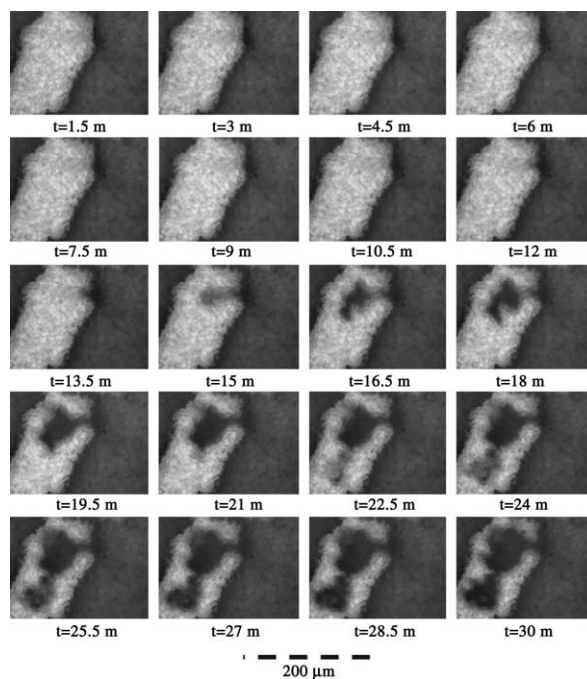


Fig. 18. Rheoscope optical micrographs of the mixing process of PCL with CL15A without shear.

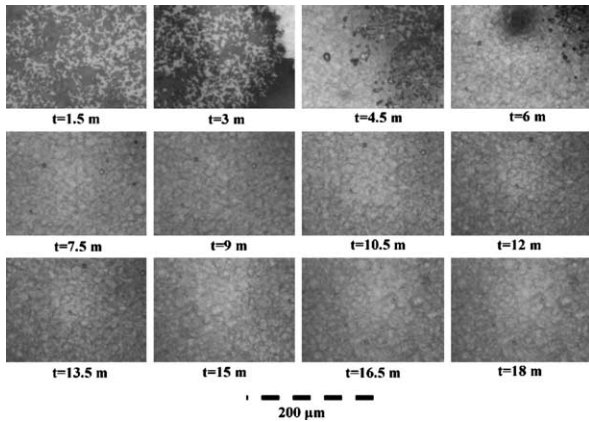


Fig. 19. Rheoscope optical micrographs of the mixing process of PCL with CL15A while shearing with 5 s^{-1} .

3.4. Overall discussion

In this section an attempt will be made to combine all observations into a complete picture on the role of the shear

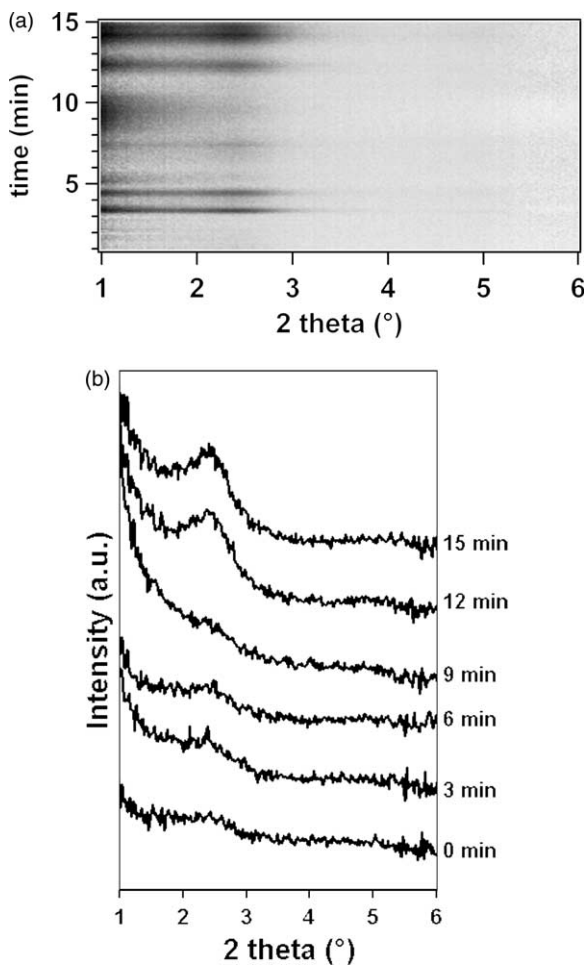


Fig. 20. SAXS patterns recorded during the mixing process of PCL with 10% CL30B without shear in the Couette shear cell as a function of scattering angle and time (a) and as a function of scattering angle for several individual times (b).

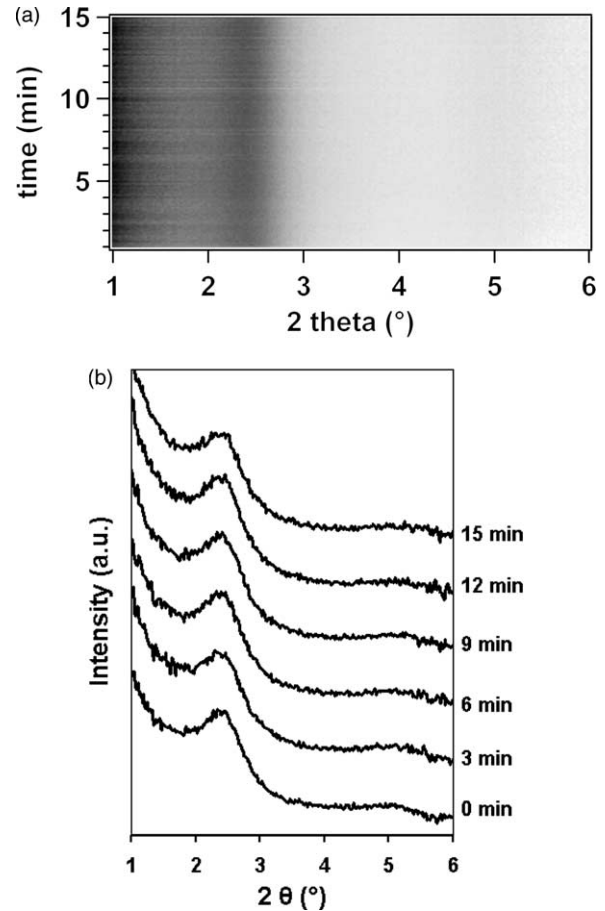


Fig. 21. SAXS patterns recorded during the mixing process of PCL with 10% CL30B while shearing with 50 s^{-1} (b) in the Couette shear cell as a function of scattering angle and time (a) and as a function of scattering angle for several individual times (b).

forces in the melt-preparation of polymer nanocomposites. The combined model for organoclay delamination as described in the introduction serves as a starting point for the discussion and its main aspects will be confronted with the results just described. The first major aspect of the model is that the final morphology is mainly determined by the chemical compatibility of the constituents and not through direct peeling of individual silicate layers from silicate layer stacks through the applied shear forces. The second major aspect of the model is that the shear forces are essential for rapid polymer nanocomposite formation because of the break up of clay agglomerates and tactoids.

When the final morphology of the different polymer clay nanocomposites studied are compared, it is immediately clear that the nanocomposites differ strongly while the melt-processing of all nanocomposites was the same. The degree of exfoliation increases from PEO, PCL, PA-12 to PA-6 nanocomposites. Also, the amount of clay tactoids that are left in the nanocomposites decreases from PEO, PCL, PA-12 to PA-6 nanocomposites. The compatibility of the clay with the specific polymer determines to a large extent the final morphology of the resulting nanocomposite. There are

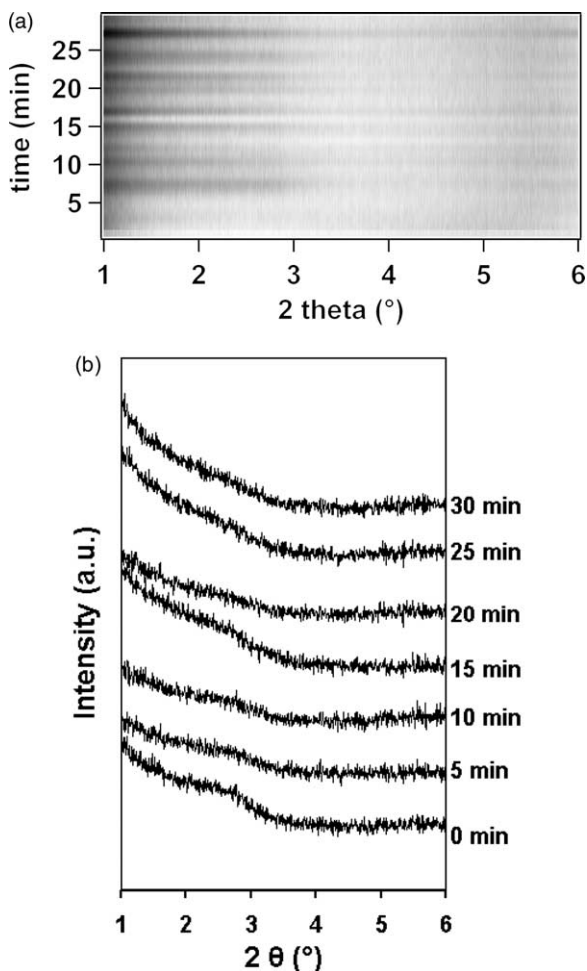


Fig. 22. SAXS patterns recorded during the mixing process of PA-12 with 5% CL30B without shear in the Couette shear cell as a function of scattering angle and time (a) and as a function of scattering angle for several individual times (b).

no indications for direct peeling of individual silicate layers from silicate layer stacks through the applied shear forces. Despite very long residence times in the extruder, the final morphologies of the resulting nanocomposites are very different. Also, the in situ XRD measurements in the Couette cell under shear showed a clear difference between the mixing of PCL and PA-12 with clay. With the mixing of PCL with clay, a partially intercalated/exfoliated morphology is reached quickly, but no further exfoliation takes place during the remaining time of the measurement. In the mixing of PA-12 with clay, the partially intercalated/exfoliated morphology is also reached quickly, but the exfoliation process continues gradually during the remainder of the measurement. The gradual exfoliation of silicate layers points strongly to the gradual break-up of the remaining clay tactoids and silicate layer stacks through the intercalation/exfoliation process by polymer chain diffusion.

However, the shear forces do play a role in the preparation of polymer nanocomposites through the second

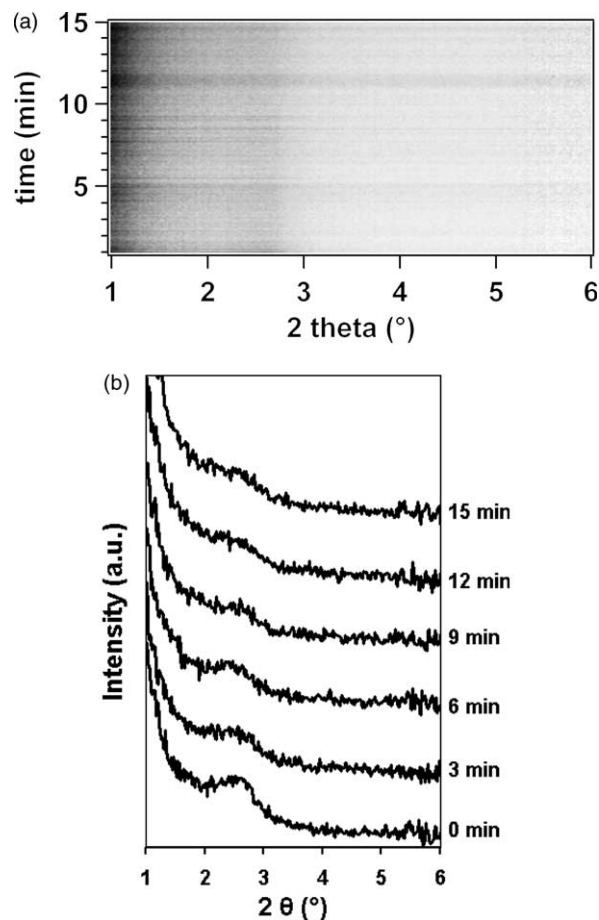


Fig. 23. SAXS patterns recorded during the mixing process of PA-12 with 5% CL30B while shearing with 50 s^{-1} in the Couette shear cell as a function of scattering angle and time (a) and as a function of scattering angle for several individual times (b).

aspect of the model. The shear forces increase the rate of organoclay delamination through the break-up of clay agglomerates and clay tactoids. The optical rheoscope measurements clearly showed the increased break-up rate of the clay tactoids under shear and the very gradual and much slower break-up without shear. Also, the observation of the melt in the Couette shear cell showed the very slow break-up of clay tactoids when shear forces are not applied. When shear forces are not applied, solely the silicate layers that are present on the clay tactoid edges are available for exfoliation. The mass transport into the primary particle was found to be a major step to nanocomposite formation. Therefore, the shear forces that are present during melt-extrusion are very important for rapid polymer nanocomposite formation. The initial break-up of agglomerates and tactoids that is provided by the shear forces is a very essential step because the exfoliation to individual silicate layers is a more gradual process. The residence time in the extruder is, therefore, also an important parameter in the preparation of polymer nanocomposites as the process to fully exfoliate the silicate layer stacks takes time. However, the elevated temperatures in the extruder are the

most important for this process and not the applied shear forces.

Summarising, the model for organoclay delamination that has been postulated is confirmed in this research. All observations confirm that the final morphology is mainly determined by the chemical compatibility between the constituents. However, break-up of clay agglomerates and tactoids through the shear forces proved to be essential for rapid polymer nanocomposite formation. A further refinement to the model is that the shear forces also play a role in the transportation of newly formed individual silicate layers away from the surface of the clay tactoids. The intercalation of silicate layers is possible when the polymer chains come into contact with silicate layer stacks. The polymer intercalation occurs as a front, which penetrates the clay tactoid from the external edge. Along the external edges, there will be large concentrations of just formed individual silicate layers. Further penetration of polymer chains towards the edges of the clay tactoid is hindered by these high concentrations. However, during melt-extrusion, the shear forces will transport the individual silicate layers away from the edges of the clay tactoid. So, the shear forces do not only have a role in the first break-up of clay agglomerates and tactoids, but also continuously homogenise the polymer/clay mixture during melt-extrusion.

4. Conclusions

The polymer/clay nanocomposites used in this paper were found to have different nanomorphologies. The PEO and PCL nanocomposites were found to have an intercalated/partially exfoliated morphology while the PA-12 and PA-6 nanocomposites were found to have highly exfoliated morphologies.

The amount of clay tactoids present in the prepared polymer nanocomposites was found to directly correlate with the degree of exfoliation. This does not seem to be an unlogical observation since the exfoliation of clay to individual silicate layers automatically means the disappearance of the clay tactoids. However, in partially exfoliated or intercalated polymer nanocomposites, non-exfoliated clay is not necessarily present as clay tactoids. Another possibility could have been that the non-exfoliated clay consists exclusively of small clay layer stacks containing only a few silicate layers, which is not the case. So, the full break-up of the tactoids is not only caused by shear forces from the extrusion process.

In the study of the break-up of μm -sized clay tactoids during melt-mixing, the following observations were done. Without applied shear forces, a gradual disappearance of the clay agglomerates was observed while with shear forces applied, a fast break-up of the clay agglomerate morphology was noticed.

In the study of the development of the nanocomposite morphology during melt-mixing, the first step to silicate

layer exfoliation, the intercalation of polymer chains between clay layer stacks, could not be observed. In the set-up of the measurement, no data could be recorded in the first 3 min. In this time, the silicate layer diffraction peak had already shifted to the lower angles of the intercalated state. However, in the mixing of PA-12 and MMT, the gradual disappearance of the mineral layer diffraction peak could be noticed after the initial shift of this peak. This is a direct measurement of slow exfoliation of mineral layers through polymer chain intercalation during shear flow. The exfoliation of silicate layer stacks to individual silicate layers was found to be a gradual process (taking about 15 min of time), even when shear forces are applied to the melt. Despite some problems, the X-ray measurements in a Couette shear cell proved to be a promising new technique to follow the exfoliation process under shear in nanocomposites in real-time.

Overall, the investigations in this paper confirm a new combined model for organoclay delamination that was postulated and researched in this paper. The shear forces in the melt-preparation of polymer layered mineral nanocomposites cause break-up of large-sized agglomerates. Further exfoliation of mineral layers is caused by polymer chain intercalation between mineral layers. The extent of further exfoliation of the mineral layers is determined by the compatibility between the polymer matrix and the mineral layers.

Acknowledgements

The authors are grateful to Jan Servaes of the KULeuven, University Technical Department, Leuven, Belgium, for the redesigning and construction of the Couette shear cell. Furthermore, the authors would like to thank the Fund for Scientific Research—Flanders (Belgium) as well as the Research Council KULeuven for the financial support of this research; one of them (B.G.), is a postdoctoral fellow of the Fund for Scientific Research—Flanders. The authors also would like to acknowledge the Dutch–Belgian Beamline (DUBBLE) research group at the ESRF, France, for their help and support with the time-resolved small angle X-ray experiments.

References

- [1] Messersmith PB, Giannelis EP. *Chem Mater* 1993;5:1064–8.
- [2] Messersmith PB, Giannelis EP. *J Polym Sci, Part A: Polym Chem* 1995;33:1047–57.
- [3] Jimenez G, Ogata N, Ogihara T. *J Appl Polym Sci* 1997;64(11):2211–20.
- [4] Vaia RA, Sauer BB, Tse OK, Giannelis EP. *J Polym Sci, Part B: Polym Phys* 1997;35:59–67.
- [5] Wang L, Schindler J, Kannewurf CR, Kanatzidis MG. *Mater Chem* 1997;7(7):1277–83.

- [6] Kim GM, Lee DH, Hoffmann B, Kressler J, Stöppelmann G. *Polymer* 2001;42:1095–100.
- [7] Hoffmann B, Kressler J, Stöppelmann G. *Abstr Pap Am Chem S* 2000; 219:286–7 [222-PMSE part 2].
- [8] Liu T, Lim KP, Tjiu WC, Pramoda KP, Chen ZK. *Polymer* 2003;44: 3529–35.
- [9] Cho JW, Paul DR. *Polymer* 2001;42:1083–94.
- [10] Lincoln DM, Vaia RA, Wang ZG, Hsiao BS. *Polymer* 2001;42: 1621–31.
- [11] Lincoln DM, Vaia RA, Wang ZG, Hsiao BS, Krishnamoorti R. *Polymer* 2001;42:9975–85.
- [12] Fu X, Qutubuddin S. *Polymer* 2001;42:807–13.
- [13] Suh DJ, Lim YT, Park OO. *Polymer* 2000;41:8557–63.
- [14] Chen TK, Tien YI, Wei KH. *Polymer* 2000;41:1345–53.
- [15] Gam KT, Sue HJ. *Abstr Pap Am Chem S* 2000;219:288–9 [222-PMSE part 2].
- [16] Fournaris KG, Karakassides MA, Petridis D. *Chem Mater* 1999;11: 2372–81.
- [17] Moussaif N, Groeninckx G. *Polymer* 2003;44:7899–906.
- [18] Giannelis EP, Krishnamoorti R, Manias E. *Adv Polym Sci* 1999;138: 107–47.
- [19] Maiti P, Nam PH, Okamoto M, Hasegawa N, Usuki A. *Macromol-ecules* 2002;35:2042–9.
- [20] Usuki A, Kojima Y, Kawasumi M, Okada A, Fukushima Y, Kurauchi T, et al. *J Mater Res* 1993;8:1175–8.
- [21] Vaia RA, Jandt KD, Kramer EJ, Giannelis EP. *Chem Mater* 1996;8: 2628–35.
- [22] Vaia RA, Giannelis EP. *Macromolecules* 1997;30:8000–9.
- [23] Dennis HR, Hunter DL, Chang D, Kim S, White JL, Cho JW, et al. *Polymer* 2001;42:9513–22.
- [24] Vaia RA, Jandt KD, Kramer EJ, Giannelis EP. *Macromolecules* 1995; 28:8080–5.
- [25] Vaia RA, Giannelis EP. *Macromolecules* 1997;30:7990–9.
- [26] Fornes TD, Yoon PJ, Hunter DL, Keskkula H, Paul DR. *Polymer* 2002;43:5915–33.
- [27] Pople JA, Hamley IW. *Rev Sci Instrum* 1998;69(8):3015–21.